applied sciences

MDPI

Article

Flexible Polyurethane Adhesives: Predictive Numerical Model Calibration through Experimental Testing at Elevated Temperature

Armando La Scala [1], Klaudia Śliwa-Wieczorek [2], Fabio Rizzo [1,*], Maria Francesca Sabbà [1] and Bogusław Zając [3]

[1] Dipartimento di Architettura Costruzione e Design, Polytechnic University of Bari, 70126 Bari, Italy; armando.lascala@poliba.it (A.L.S.); mariafrancesca.sabba@poliba.it (M.F.S.)
[2] Division of Bridge, Metal and Timber Structures, Faculty of Civil Engineering, Cracow University of Technology, 31-155 Cracow, Poland; klaudia.sliwa-wieczorek@pk.edu.pl
[3] Division of Geotechnics and Strength of Materials, Faculty of Civil Engineering, Cracow University of Technology, 31-155 Cracow, Poland; boguslaw.zajac@pk.edu.pl
* Correspondence: fabio.rizzo@poliba.it

Abstract: The thermo-mechanical behavior of polyurethane adhesive joints in wood structures is a crucial aspect that needs to be understood to ensure the durability and safety of timber structures, especially in seismic regions. As mass timber, particularly cross-laminated timber, continues to gain popularity as a building material, it is important to pay special attention to the behavior of connections between the timber elements. The use of flexible polyurethane adhesives presents a promising alternative to conventional mechanical connections in seismic-resistant timber structures. This research highlights the potential of polyurethane-based joints at elevated service temperature, offers a promising alternative to traditional wood joints, and suggests viability for post-fire restoration of wood structures. The response at the interface between wood and polyurethane under flexural stresses is also evaluated, underscoring the broader application possibilities of flexible adhesives in wood construction for mechanical and physical improvements.

Keywords: elevated temperature; flexible adhesives; polyurethane; wood; numerical analysis

check for updates

Citation: La Scala, A.; Śliwa-Wieczorek, K.; Rizzo, F.; Sabbà, M.F.; Zając, B. Flexible Polyurethane Adhesives: Predictive Numerical Model Calibration through Experimental Testing at Elevated Temperature. *Appl. Sci.* **2024**, *14*, 1943. https://doi.org/10.3390/app14051943

Academic Editor: Stefano Invernizzi

Received: 30 January 2024
Revised: 19 February 2024
Accepted: 21 February 2024
Published: 27 February 2024

Copyright: © 2024 by the authors. Licensee MDPI, Basel, Switzerland. This article is an open access article distributed under the terms and conditions of the Creative Commons Attribution (CC BY) license (https://creativecommons.org/licenses/by/4.0/).

1. Introduction

Cross-laminated timber (CLT) is a popular construction material due to its high stiffness, shear, tension and in-plane compression strength, as well as its limited ductility and energy dissipation capacity. The connections between individual CLT elements are crucial to the ductility and energy dissipation of wood structures, ensuring sufficient stiffness and strength between structural elements. During an earthquake, the behavior of CLT buildings is mainly affected by the performance of connections between adjacent panels and other structural elements. Therefore, for these structural types, the main risk zones during exceptional stresses are concentrated at nodes and joints. The mechanical performance of these connections is affected by several factors, such as wood species, adhesive types, and joint design. In recent years, polyurethane adhesives have gained popularity for their excellent bonding properties and compatibility with wood materials [1–5]. Polyurethane is a commonly used material in the construction industry due to its excellent thermal insulation properties [1,6]. Epoxy adhesives are already commonly used to bond steel bars, sheet metal or fiber-reinforced polymer composites in the most stressed areas of a building for reinforcement purposes [7–9]. Flexible adhesives, on the other hand, are used for repairing masonry and concrete structures and for seismic protection of buildings [10–12]. The durability of adhesive joints is affected by several factors, including materials, stresses, and environment. Vallée et al. [13] conducted studies on double-overlap joints consisting of glass fiber elements (GFRP) and polyurethane adhesives, defining the increase in strength as a function of the increase in joint thickness. Liao et al. [14] analyzed the impact of adhesive layer thickness and joint angle on the behavior of a biesau adhesive joint and

found that the fracture energy of brittle adhesives increases as adhesive layer thickness decreases. The impact of moisture and temperature on adhesive properties has also been studied [15–17]. Moussa et al. [18] observed the impact of cyclic heating and cooling on epoxy resins and found that mechanical properties were restored or even improved after cooling. Adhesive joints operating at elevated temperatures were studied by [19], who found that flexible joints reduced stress concentrations and redistributed stresses over a larger area. Several models have also been developed to estimate the stress distribution in adhesive layers, considering factors such as the deformation of bonded components, bending moment and large strains [20]. Da Silva et al. [21,22] provided a detailed review of analytical models for adhesive joints and concluded that the design process must consider geometry, temperature, and type of analysis.

However, the in situ thermo-mechanical behavior of polyurethane joints in wood structures has not been extensively studied. To fill this knowledge gap, this study aims to investigate the thermo-mechanical behavior of polyurethane joints in wood buildings. The study will examine the effects of temperature on the performance of polyurethane joints in wooden elements, focusing on their durability and ability to maintain physicochemical properties under thermal degradation.

Polyurethane joints in wood buildings exhibit an interesting thermo-mechanical behavior that makes them useful for post-fire interventions [6,12,23–27]. When exposed to high temperatures, as in fire, the bond strength of polyurethane joints remains sufficiently stable [27,28]. This is due to the excellent thermal stability and resistance to degradation of polyurethane materials. Kwiecień et al. [29] confirmed resistance of a single polyurethane material (used in this study in research) against various ageing factors, showing also that it presents stable properties in elevated temperatures up to 200 °C. However, it is critical to understand the limits and potential damage modes of polyurethane joints in wood buildings under different temperature conditions [30,31].

For the design of new wood buildings, the introduction of these new types of polyurethane joints is important because they offer several advantages over traditional adhesive joints [32,33]. The flexibility of polyurethane joints allows for greater movement and deformation, which is particularly beneficial in wood structures that experience changes in moisture and temperature [16,34]. This flexibility helps to reduce the stress concentration at the joint interface and improve the overall performance of the structure. In addition, studies have found that polyurethane joints have greater shear strength, elastic stiffness, and strength degradation capability than mechanical fasteners commonly used in wood buildings [35–37]. Considering the advantages of polyurethane joints in terms of thermal stability and mechanical properties, they can also be a viable solution for post-fire interventions aimed at restoring the structural integrity of a wooden structure.

The characteristics of flexible adhesives indicate application possibilities in the field of wood construction for both mechanical and physical improvements. The objective of this work is to identify the potential of flexible polyurethane-based connections in the special case of operation at elevated temperatures (which can occur during normal use of structures as a result of seasonal changes or exposure of the components to sunlight, e.g., in transparent roof structures), as an alternative to traditional wood connections. In addition, the study will evaluate the response at the interface between wood and polyurethane in the case of flexural stresses.

2. Experimental Test

The purpose of the experimental program was to investigate the impact that an increase in temperature had, not only on the load-bearing capacity of the laminated beams, but also on the deflection under the action of the applied load. In addition, the influence of adhesive layer thickness on the structural response of the joint at four different temperatures, 20 °C, 40 °C, 60 °C and 80 °C, was investigated. For this experimental program, a three-point bending test was performed on six wooden laminated beams at each temperature and for each thickness (t = 1, 2 and 4 mm). A total of 72 laminated beams were tested. The

data obtained from the three-point bending test were then compared with those from a finite element model of the laminated beams considered. The test specimens were made as composite beams consisting of Douglas fir wood layers and Sika PS-type flexible polyurethane layers with different thicknesses (1 mm, 2 mm and 4 mm). The resulting specimens were subjected to bending tests at elevated temperatures (20, 40, 60 and 80 °C), during which load capacity and deflection were measured.

2.1. Materials

Each laminated composite beam was constructed using a combination of two single Douglas fir (Pseudotsuga menziesii) lamellas, each with a cross-sectional area of 40 mm by 20 mm. Sika PS flexible polyurethane adhesive was used for bonding in three different configurations, with varying thicknesses of t = 1, 2 and 4 mm.

The average modulus of elasticity of wood was calculated at temperatures of 20 °C, 40 °C, 60 °C and 80 °C. The results are shown in Table 1 with corresponding ratio related to parameters at 20 °C. They indicate that wood properties change in elevated temperatures, dropping even to 22% at 80 °C.

Table 1. Elastic modulus of wood experimentally measured.

Young Modulus E (MPa)/(Ratio (−))			Shear Modulus G (MPa)/(Ratio (−))		
E_x	E_y	E_z	G_{xy}	G_{xz}	G_{yz}
20 °C					
10611 (1.00)	531 (1.00)	531 (1.00)	757.9 (1.00)	757.9 (1.00)	75.8 (1.00)
40 °C					
9761 (0.92)	488 (0.92)	488 (0.92)	697.2 (0.92)	697.2 (0.92)	69.7 (0.92)
60 °C					
8763 (0.83)	438 (0.82)	438 (0.82)	625.9 (0.83)	625.9 (0.83)	62.6 (0.83)
80 °C					
8334 (0.78)	417 (0.78)	417 (0.78)	595.3 (0.78)	595.3 (0.78)	59.5 (0.78)

2.2. Test Setup

Bending tests measure the behavior of a beam subjected to different loading conditions. They are commonly performed on relatively flexible materials such as polymers, wood and composite materials. At its most basic level, a bending test is performed on a universal testing machine by placing a specimen on two supporting anvils and bending it through a force applied through one or two loading anvils to measure its properties. In the three-point bending test, it balances a specimen between two lower supports while a force centered in the middle is applied by the testing machinery. The uniform stress area is quite small and concentrated below the center point of loading. Different testing standards may require anvils to be fixed, rotated or oscillating. Specifically, the standards governing the performance of these tests are ISO 13061-3, ISO 13061-4 and ASTM D143 [38–40]. The standards listed above are the most used wood bending tests, but there are many other wood testing standards in various standards bodies, including ASTM, ISO, EN, BS, JAS and JIS.

Three sets of tests (6 samples for each joint thickness) were performed for all four temperature levels, for a total of 72 samples. The beams consisted of two single lamellas with a cross-sectional area of 40 × 20 mm and a length of 420 mm (see Figure 1c). The spacing between the supports was 350 mm. A PTS (model PT 100) thermocouple sensor (VISHAY Electronic GmbH, Selb, Germany) was used to measure the temperature inside the adhesive layer. Due to its small dimensions of 0.45 × 0.85 × 1.55 mm, this sensor did not disturb the obtained results. The load was applied according to the displacement-controlled method through a Zwick Roell 1455 universal testing machine (UTM), with a

load head movement speed of 10 mm/min. Specimens were instrumented with a Linear Variable Displacement Transducer (LVDT) mounted at the center of the beam to measure the displacement. The test stand is presented in Figure 1a.

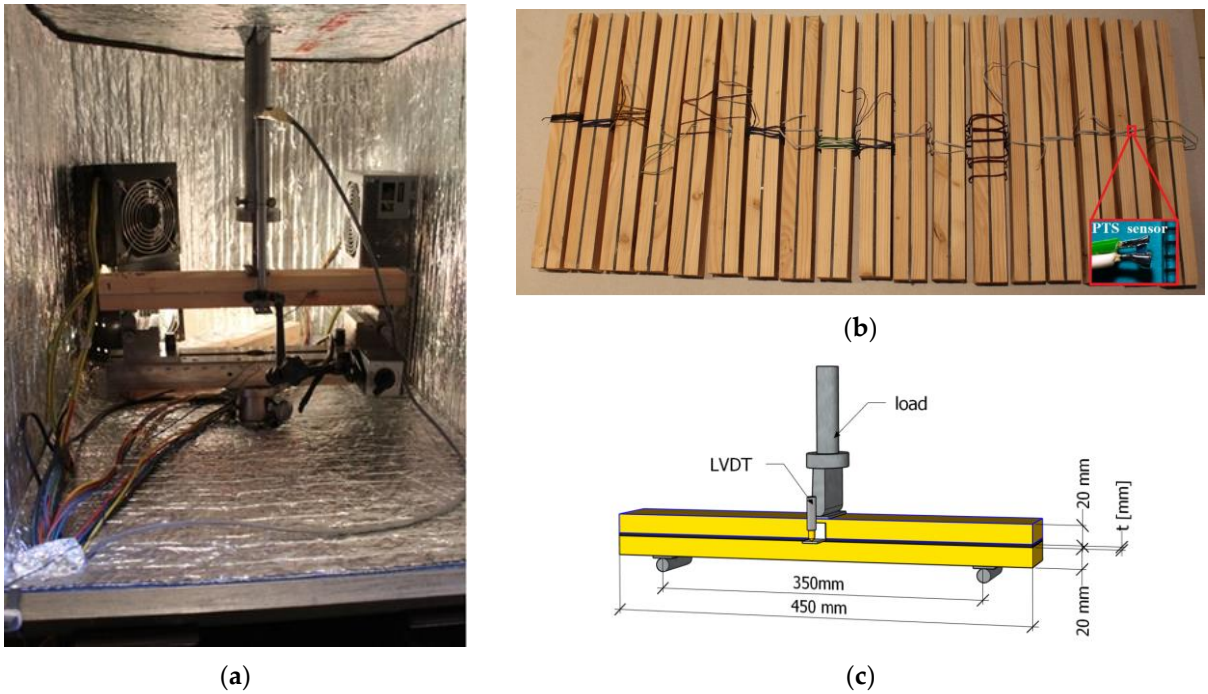

(**a**) (**b**) (**c**)

Figure 1. The test set-up: view of the beam on the test bench in the temperature chamber (**a**), view of selected samples with PT100 temperature measurement sensor (**b**) and schematic view, where t—adhesive layer thickness (**c**).

Before testing, all specimens were cured for 21 days in a room with a stable temperature of 20 °C and humidity of 65% ± 5%. The adhesive was mixed as described in the product data sheet. The mixing ratio for Sika PS A:B = 100:11 parts by weight. The adhesive was mixed for 60–80 s, and the mechanical mixing speed was 600–800 rpm.

2.3. Experimental Results

The results revealed a non-linear behavior of flexible adhesives, characterized by advantageous reduction of stress concentration and uniform stress distribution along the bond line. Based on the data obtained, several characteristic parameters of the specimens were identified.

The results of bending tests on the laminated beams were analyzed. The impact of temperature and adhesive layer thickness on joint load capacity was described. Types of failure were described for each beam according to the EN ISO 10365:1992 standard [41], using the following designations: cohesive failure in wood (ct), cohesive failure in polymer (cp), adhesive failure at the wood–polymer interface (at-p), and mixed failure (md). The maximum force value (F_{max}) and corresponding displacement (dL/F_{max}) were recorded with LVDT sensor placed in the mid-span of the beam. Table 2 shows the average values of maximum force μ_{Fmax} and corresponding displacement $\mu_{\delta max}$ for the 6 specimens for each adhesive layer thickness and each temperature. The coefficients of variation were calculated (shown in brackets). The initial elastic stiffness K was determined for the range from 0.1 F_{max} to 0.4 F_{max} (the same procedure is used to determine the flexural modulus of wood according to EN 408:2012 [42]). A linear regression analysis of the measured deflections was performed; coefficients of determination (R^2) greater than 0.99 were taken.

Table 2. Results of the bending test.

SAMPLE TYPE (THICKNESS OF THE ADHESIVE LAYER)		TEST TEMPERATURE (°C)			
		20	**40**	**60**	**80**
PS 1 mm Failure type (cp)		**Force**			
	$\mu_{F_{max}}$ (kN)	9.39 (1.00)	7.61 (0.81)	6.26 (0.67)	5.76 (0.61)
		Displacement			
	$\mu_{\delta_{max}}$ (mm)	11.4 (1.00)	10.4 (0.92)	9.3 (0.86)	7.9 (0.69)
		Initial elastic stiffness			
	K (N/mm)	849.0 (5.6)	748.4 (4.2)	805.5 (11.2)	795.0 (7.2)
PS 2 mm Failure type (cp)		**Force**			
	$\mu_{F_{max}}$ (kN)	9.34 (1.00)	7.03 (0.75)	5.84 (0.62)	5.25 (0.56)
		Displacement			
	$\mu_{\delta_{max}}$ (mm)	11.4 (1.00)	9.9 (0.87)	7.7 (0.67)	7.7 (0.67)
		Initial elastic stiffness			
	K (N/mm)	780.7 (7.2)	838.8 (6.7)	824.7 (3.2)	767.5 (4.6)
PS 4 mm Failure type (cp)		**Force**			
	$\mu_{F_{max}}$ (kN)	9.41 (1.00)	7.80 (0.83)	6.27 (0.67)	5.50 (0.58)
		Displacement			
	$\mu_{\delta_{max}}$ (mm)	13.7 (1.00)	11.0 (0.80)	9.7 (0.71)	9.1 (0.66)
		Initial elastic stiffness			
	K (N/mm)	789.0 (5.9)	783.1 (5.9)	881.7 (4.1)	786.5 (9.3)

Bending test results for all specimens are presented as force-displacement diagrams for the chosen specimens (t = 1, 2 and 4 mm) at four temperature values. The results are presented in Figure 2.

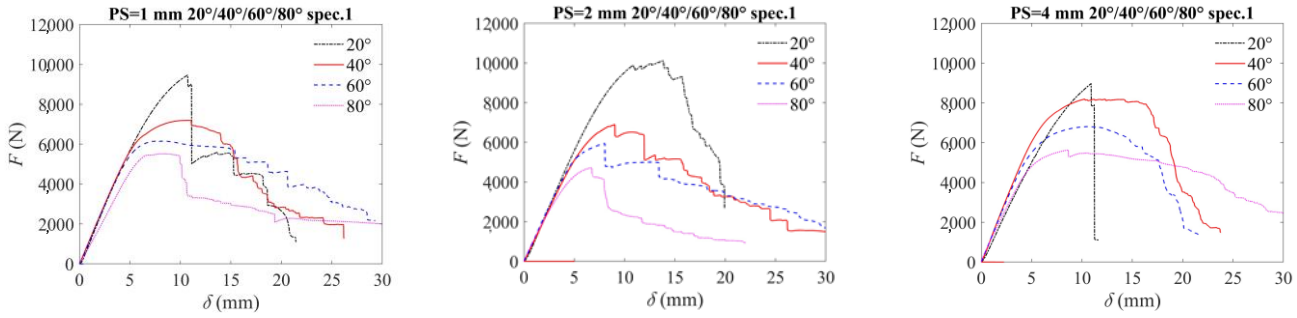

Figure 2. Force-displacement graphs: adhesive layer thickness t = 1 mm (**a**); adhesive layer thickness t = 2 mm (**b**); adhesive layer thickness t = 4 mm (**c**).

The average breaking force at 20 °C, depending on the adhesive layer thickness (t), was 9.39 kN for t = 1 mm, 9.34 kN for t = 2 mm and 9.41 kN for t = 4 mm, respectively. When the temperature increased to 80 °C, the force decreased to the following values: 5.76 kN for t = 1 mm, 5.25 kN for t = 2 mm and 5.50 kN for t = 4 mm, which were: 61%, 56% and 58% of the destructive force at 20 °C, respectively (Table 2). Similar relation was observed in the case of ultimate displacement, where the temperature increases to 80 °C caused a drop in values to: 7.9 mm for t = 1 mm, 7.7 mm for t = 2 mm and 9.1 mm for t = 4 mm, which were almost equal: 69%, 67% and 66% of the ultimate displacement at 20 °C, respectively

(Table 2). The effect of adhesive thickness did not seem so pronounced, and the differences between the mean values (F_{max}) of the 1-, 2- and 4-mm thicknesses were within 1% at 20 °C. However, the corresponding displacements were significantly higher for adhesive thickness of t = 4 mm than for t = 1 and 2 mm (17% difference). The results clearly show that flexible bonding does not show a decrease in initial elastic stiffness K with increasing temperature up to 80 °C (the slope of the curve is almost constant)—Figure 2. This observation is very promising for design procedure, because the use of safety factors of around 0.5 gives stable properties in the whole range of the considered elevated temperatures (up to 80 °C). As can be seen from Table 2, the differences between the highest and lowest average values of initial elastic stiffness (from the range 0.1 F_{max} to 0.4 F_{max}) are respectively:

- for t = 1 mm → 100.6 N/mm;
- for t = 2 mm → 71.5 N/mm;
- for t = 4 mm → 98.6 N/mm.

It can be concluded that flexible polyurethane adhesives are stable at high temperatures up to 80 °C. The plastic form of damage is clearly visible for laminated beams with an adhesive thickness of 4 mm. The failure of the composite beam was triggered by a crack formed in the adhesive layer. Immediately following this, in fact, a sudden delamination occurred in the shear span (the span between a point load and the nearest support). As the load increased, the cracking propagated into the lower layer, where the damage occurred in the wood plank due to the tensile stresses along the fiber being exceeded.

3. Finite Element Model

The present work is aimed at studying and understanding the interaction between wood and polyurethane in a transient thermal regime. The experimental test conducted provided a certain amount of data, from which it was possible to calibrate a finite element model, made according to the principle of micro-modeling. In this case, in fact, each element was represented in the numerical environment by means of solid "brick" elements, totally corresponding in geometry and mechanical properties to the real materials.

The greatest difficulty was presented by the need to precisely describe the damage model of the materials present; in this case, for wood, reference was made to the "plastic damage" already present in the software, while for polyurethane, this being a viscoelastic material, it was necessary to take into account the hysteretic effects by means of the description of the so-called "Mullins effect".

Among the different types of joints experimentally analyzed, the case corresponding to the 4-mm polyurethane layer was chosen to be modeled in Abaqus/CAE v.2017. This choice was necessary because the results for the smaller thicknesses were partly affected by the mesh size. In fact, small thicknesses require a generic finite element size, which is too small compared to the solver's capabilities, for which the computational burden increased exponentially.

The need to introduce an FE model stems from the possibility of extending the case study and, more importantly, the possibility of monitoring variability of parameters that would otherwise be difficult to estimate in the field.

Model Description

The model was built in Abaqus/CAE 2017 by resorting to brick-type elements for each layer of the beam. The finite element type adopted is C3D8RH, usually used for purely mechanical analysis, with a total of 16,269 nodes and 10,752 elements. The elements comprising the model are defined as deformable elements with associated non-linearity and cracking characteristics. Material-related constitutive non-linearities were simulated by defining appropriate constitutive bonds: anisotropic elasto-plastic for wood and Yeoh-like hyperelastic for polyurethane.

An elasto-plastic constitutive bond was adopted for wood boards, in which the anisotropy of the material in the three main directions was considered. Linear elasticity in an orthotropic material is most easily defined by giving the "engineering constants":

the three moduli E_1, E_2, E_3; Poisson's ratio ν_{12}, ν_{13}, ν_{23}; and the shear moduli G_{12}, G_{13}, and G_{23} associated with the principal directions of the material. These moduli define the elastic yielding according to:

$$\begin{Bmatrix} \varepsilon_{11} \\ \varepsilon_{22} \\ \varepsilon_{33} \\ \gamma_{12} \\ \gamma_{13} \\ \gamma_{23} \end{Bmatrix} = \begin{bmatrix} 1/E_1 & -\nu_{21}/E_2 & -\nu_{31}/E_3 & 0 & 0 & 0 \\ -\nu_{12}/E_1 & 1/E_2 & -\nu_{32}/E_3 & 0 & 0 & 0 \\ -\nu_{13}/E_1 & -\nu_{23}/E_2 & 1/E_3 & 0 & 0 & 0 \\ 0 & 0 & 0 & 1/G_{12} & 0 & 0 \\ 0 & 0 & 0 & 0 & 1/G_{13} & 0 \\ 0 & 0 & 0 & 0 & 0 & 1/G_{23} \end{bmatrix} \begin{Bmatrix} \sigma_{11} \\ \sigma_{22} \\ \sigma_{33} \\ \sigma_{12} \\ \sigma_{13} \\ \sigma_{23} \end{Bmatrix} \quad (1)$$

The quantity ν_{ij} has the physical interpretation of Poisson's ratio that characterizes the transverse deformation in the j direction when the material is stressed in the i direction. In general, ν_{ij} if it is not equal to ν_{ji}: is related by $\nu_{ij}/E_i = \nu_{ji}/E_j$. Engineering constants can also be given as functions of temperature and other predefined fields, if necessary.

The elastic solution must meet the following stability conditions:

$$\begin{aligned} &E_1, E_2, E_3, G_{12}, G_{13}, G_{23}, > 0, \\ &|\nu_{12}| < (E_1/E_2)^{1/2}, \\ &|\nu_{13}| < (E_1/E_3)^{1/2}, \\ &|\nu_{23}| < (E_2/E_3)^{1/2}, \\ &1 - \nu_{12}\nu_{21} - \nu_{23}\nu_{32} - \nu_{31}\nu_{13} - 2\nu_{21}\nu_{32}\nu_{13} > 0 \end{aligned} \quad (2)$$

When the left side of the inequality approaches zero, the material exhibits incompressible behavior. Using the relations $\nu_{ij}/E_i = \nu_{ji}/E_j$, the second, third and fourth restrictions of the previous series can also be expressed as:

$$\begin{aligned} &|\nu_{21}| < (E_2/E_1)^{1/2}, \\ &|\nu_{31}| < (E_3/E_1)^{1/2}, \\ &|\nu_{32}| < (E_3/E_2)^{1/2}. \end{aligned} \quad (3)$$

The following Tables 3 and 4 show the parameters defined in the FE model for the representation of wooden planks.

Table 3. Mechanical parameters of wood.

Elastic Behavior of Wood		
E_1 (MPa)	390	Stamer et al., 1935 [43,44]
E_2 (MPa)	690	
E_3 (MPa)	15,900	
ν_{12}	0.25	
ν_{13}	0.01	
ν_{23}	0.03	
G_{12} (MPa)	36	
G_{13} (MPa)	770	
G_{23} (MPa)	620	

Table 4. Post-elastic characteristic of wood.

Plastic Behavior of Wood		
σ_y (MPa)	104	parametric

Yeoh's model, in which the material is defined as hyperelastic isotropic, was adopted for the polyurethane layer. According to this phenomenological model, the elastic characteristics of rubber can be represented by a strain energy density function, which is a series

of powers of the strain invariants I_1, I_2 and I_3 of the Cauchy–Green strain tensors. This consideration was the basis of Ronald Rivlin's theory, from which Yeoh's model starts. In Yeoh's model, the only variable that is considered is I_1 in the case where the material is assumed to be incompressible. In the case of hyperelastic compressible materials, the dependence on I_3 is added. Because only one of the three invariants of the Cauchy–Green strain tensor is considered, Yeoh's model is sometimes called a reduced polynomial model. This is because the strain energy density function is represented by a polynomial. In ABAQUS, hyperelastic materials are described in terms of the "strain energy potential", which defines the strain energy stored in the material per unit reference volume (volume in the initial configuration) as a function of the strain at that point in the material. Several forms of strain energy potentials are available in ABAQUS to model approximately incompressible isotropic elastomers [45].

The form of the Yeoh strain energy potential is:

$$U = C_{10}(\bar{I}_1 - 3) + C_{20}(\bar{I}_1 - 3)^2 + C_{30}(\bar{I}_1 - 3)^3 + \frac{1}{D_1}(J^{el} - 1)^2 + \frac{1}{D_2}(J^{el} - 1)^4 + \frac{1}{D_3}(J^{el} - 1)^6 \quad (4)$$

where U is the strain energy per unit reference volume, and C_{i0} and D_i are temperature-dependent material parameters; it is the first deviatoric strain invariant defined as:

$$\bar{I}_1 = \bar{\lambda}_1^2 + \bar{\lambda}_2^2 + \bar{\lambda}_3^2 \quad (5)$$

where deviatoric traits $\bar{\lambda}_i = J^{-\frac{1}{3}}\lambda_i$; J is the total volume ratio; and J^{el} is the elastic volume ratio that relates to the total volume ratio J and the thermal volume ratio J^{th}, according to:

$$J^{el} = \frac{J}{J^{th}} \quad (6)$$

with J^{th} in turn defined as:

$$J^{th} = (1 + \varepsilon^{th})^3 \quad (7)$$

where ε^{th} is the linear thermal expansion strain obtained from the temperature and isotropic thermal expansion coefficient.

The λ_i, finally, are the main stretches. The initial shear modulus and bulk modulus are given by:

$$\mu_0 = 2C_{10} \qquad K_0 = \frac{2}{D_1} \quad (8)$$

A convenient way to define a hyperelastic material is to provide ABAQUS with data from experimental tests [45]. ABAQUS then calculates the constants by a least-squares method. The experimental tests for which ABAQUS can fit the data are:

- Uniaxial tension and compression.
- Equi-biaxial tension and compression.
- Planar tension and compression (pure shear).
- Volumetric tension and compression.

Thus, Yeoh parameters were calculated in ABAQUS as C10 = −2.977 MPa and C20 = −2.812 MPa, based on uni-axial tensile test curves carried out at room temperature; the values of nominal stress and strain considered are shown in Table 5.

A further investigation using ABAQUS calculation has been computed by assuming that another compressible hyperelastic Mooney–Rivlin (M–R) model was applied after [46] in form (9). M–R parameters, determined in ABAQUS for different temperature curves of the uni-axial tensile test of polyurethane PS, are listed in Table 6 and were used in further numerical analysis.

$$W = C_{10}(\bar{I}_1 - 3) + C_{01}(\bar{I}_2 - 3) + \frac{1}{D_1}\left(J^{el} - 1\right)^2 \quad (9)$$

Table 5. Yeoh parameters for polyurethane PS in various temperatures.

Uniaxial Tests for Determination of Hyperelastic Parameters of Polyurethane		
Nominal stress	Nominal strain	
0.022	0	Pecnik et al. [46]
0.938	0.05	
1.555	0.1	
1.984	0.15	
2.257	0.2	
2.4316	0.25	
2.531	0.3	

Table 6. Mooney–Rivlin stresses for polyurethane PS at various temperatures.

PS (°C)	C01 (MPa)	C10 (MPa)	D1 (kPa^{-1})
20	1.451	−0.464	4.6×10^{-6}
40	1.448	−0.461	4.6×10^{-6}
60	1.436	−0.459	4.6×10^{-6}
80	1.428	−0.457	4.6×10^{-6}

4. Results

Several FE models were constructed in ABAQUS, one for each temperature level achieved during the experimental phase for the polyurethane adhesive thickness t = 4 mm. The models obtained were calibrated based on data from the laboratory tests carried out, with extremely satisfactory results; in fact, the curves found by numerical analysis showed a deviation of less than 10% for each of the cases observed.

The use of the Finite Element Method in modeling made it possible to calibrate the numerical models using the experimental results, providing a visual representation of the structural flexibility and the promising properties manifested by structural elements made with the coupling of wood and flexible adhesives. The main objective of this research is to develop an innovative and advantageous wood adhesive technology compared to conventional systems that employ rigid and thin layers of adhesives.

Figures 3–6 show the calibration results for each model, compared with the different curves from the experimental tests at considered temperatures. The stress measure used in Abaqus is the Cauchy or "true" stress, which is the force per unit area. In this case, we present the results in terms of principal stresses to show what the load path is and how the forces are distributed within the composite beam.

The reliability of the models, demonstrated by calibration on the experimental data, allowed for the development of considerations of quantities and phenomena that had not been possible to observe during the experimental phase.

ABAQUS/Standard offers several contact formulations. Each formulation is based on the choice of a contact discretization, a tracking approach, and the assignment of "master" and "slave" roles to the contact surfaces. The software defines incremental relative motion (also known as slip) as the scalar product of the incremental relative nodal displacement vector and a local tangent direction. The incremental relative nodal displacement vector measures the motion of a slave node relative to the motion of a master surface. Incremental slip is accumulated only when the slave node is in contact with the master surface. The sums of all these incremental slips during the analysis are reported as CSLIP1 and CSLIP2 [45].

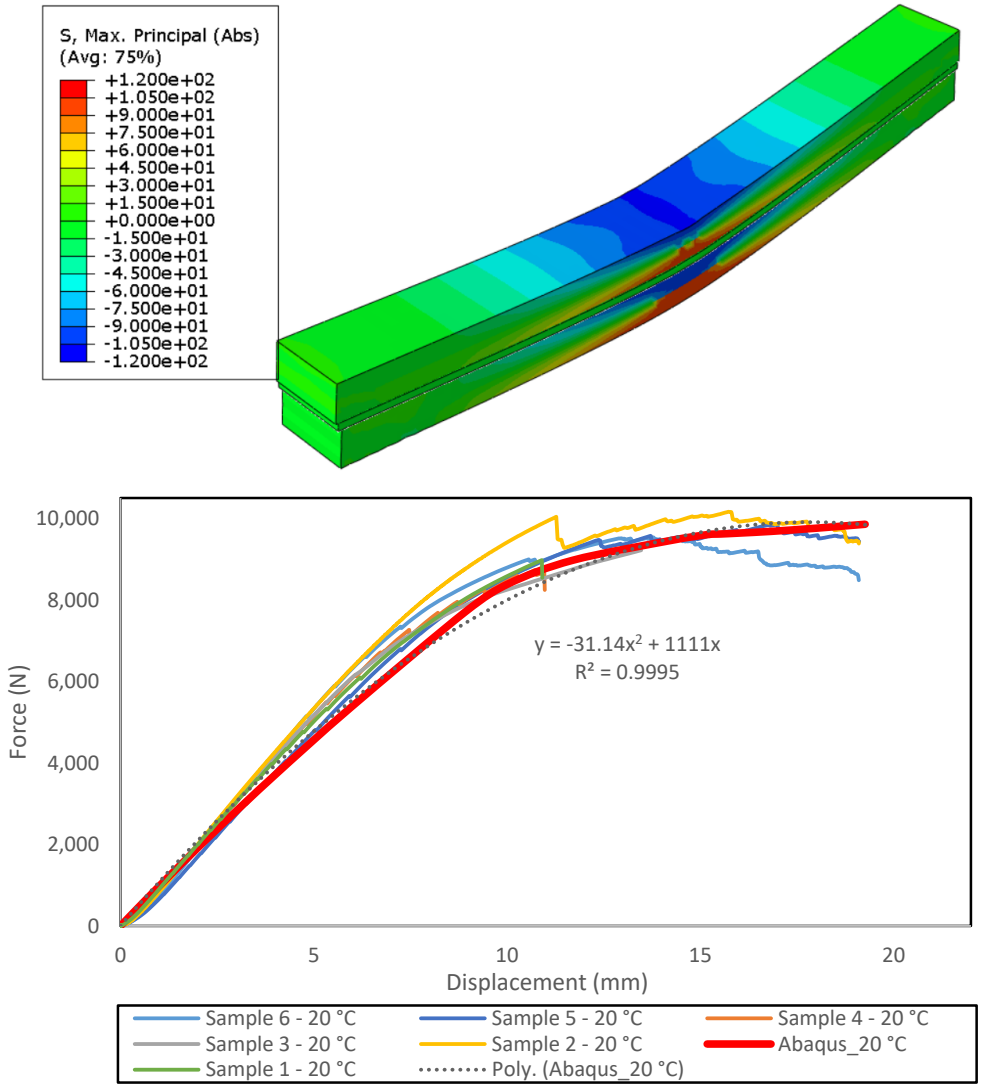

Figure 3. Numerical simulation of the bending test at 20 °C; comparison of numerical result and experimental data in terms of force-displacement.

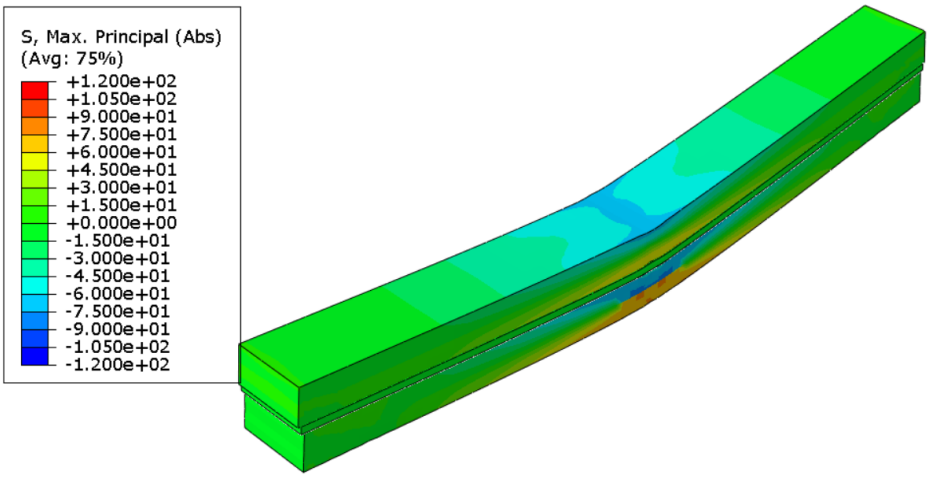

Figure 4. *Cont.*

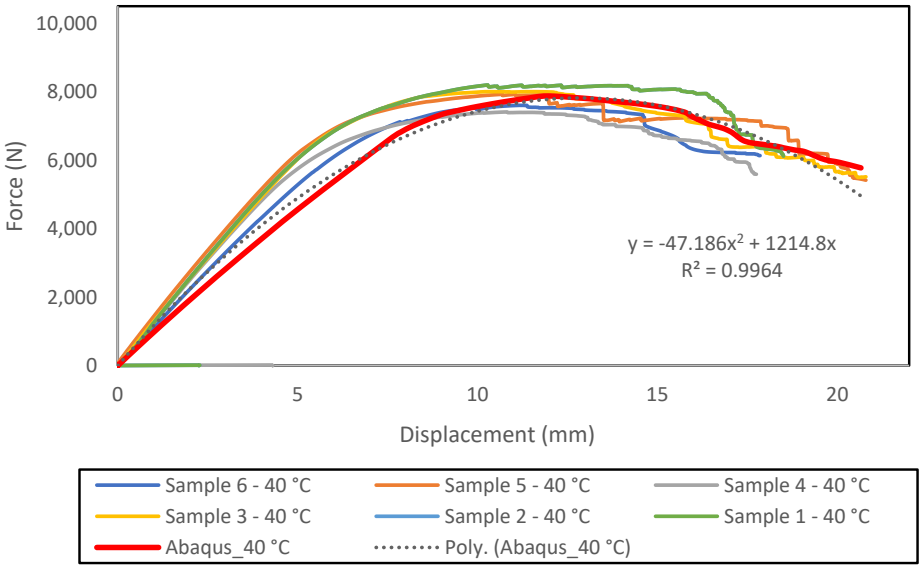

Figure 4. Numerical simulation of the bending test at 40 °C; comparison of numerical result and experimental data in terms of force-displacement.

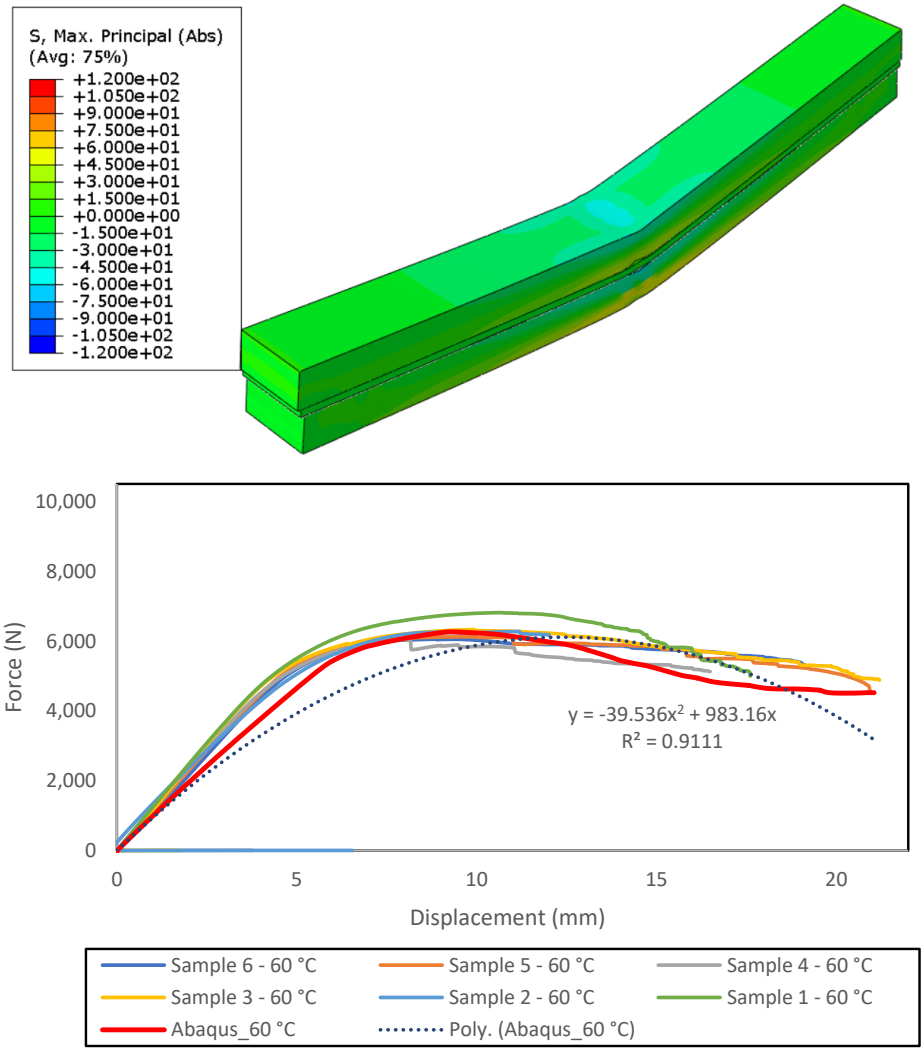

Figure 5. Numerical simulation of the bending test at 60 °C; comparison of numerical result and experimental data in terms of force-displacement.

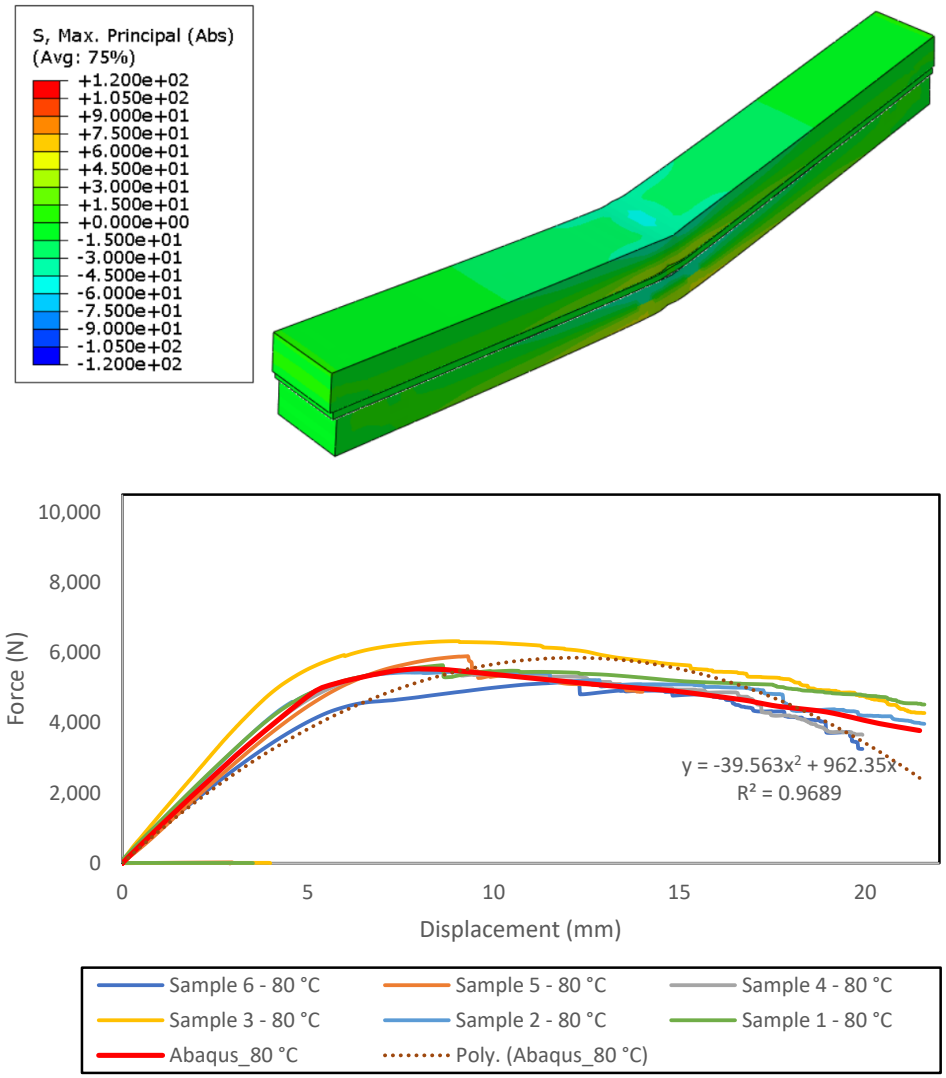

Figure 6. Numerical simulation of the bending test at 80 °C; comparison of numerical result and experimental data in terms of force-displacement.

The accumulated slip at a slave node (CSLIP) can provide a good estimate of how much a slave node has moved. Contact tensions, on the other hand, are defined by CPRESS, which is calculated as the net normal contact force per unit area, and CSHEAR, which is the tangential stress in the two directions x and z (in the 3D case) per unit area.

The logarithmic strain, LE, is:

$$\varepsilon^L = \ln \boldsymbol{V} = \sum_{i=1}^{3} ln\lambda_i \boldsymbol{n}_i \boldsymbol{n}_i^T \tag{10}$$

where $\boldsymbol{V} = \sqrt{\boldsymbol{F} \cdot \boldsymbol{F}^T}$ is the left stretch tensor, $\boldsymbol{F}$ is the deformation gradient, λ_i are the principal stretches, and $\boldsymbol{n}_i$ are the principal stretch directions in the current configuration. This is the strain output for hyperelastic materials. The three output variables obtained from the software, CPRESS, CSHEAR and CSLIP, represent the attritive behavior at the interface between two surfaces. This allows precise analysis of the behavior at the contact zones between wood and polyurethane.

In Figures 7–10, the contact pressure (CPRESS), contact shear stress (CSHEAR), and relative slipping between the polyurethane and the wood (CSLIP) are shown at the end of the test. The images show the evolution of the stress state at the wood/polyurethane interface (CPRESS and CSHEAR) with increasing temperature. The heating strongly affects

the normal stresses, which decrease significantly due to the softening of the polyurethane. The shear stresses in the principal sliding direction also decrease, confirming the weakening of the bonds between the polyurethane polymer chains with increasing temperature. However, there was no consistent pattern in the mutual slip between the surfaces of the interface (CSLIP). Variations of 2 to 2.5 mm were observed, but there was no discernible trend of increase or decrease. To better evaluate this condition, deformations (LE) were also observed. In this case, the strain values (in absolute value) increase from 0.02 to 0.10 as the temperature rises. For brevity, the results are shown relative to the top interface surface only.

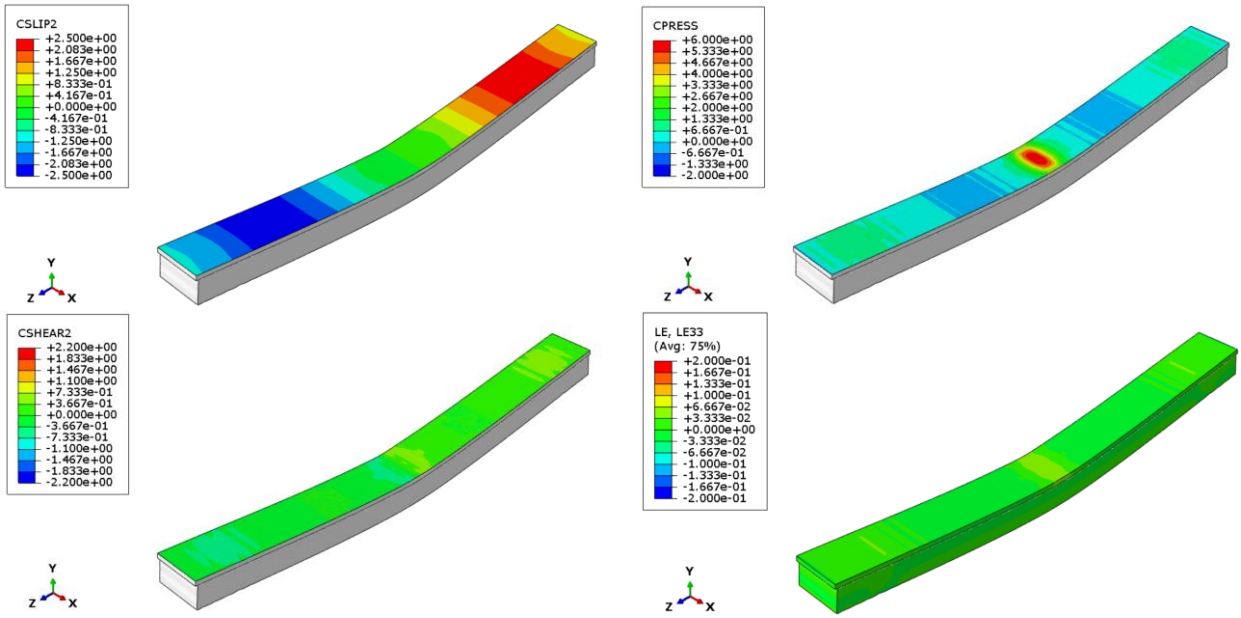

Figure 7. Trends for CSLIP, CPRESS, CSHEAR and strain values at 20 °C.

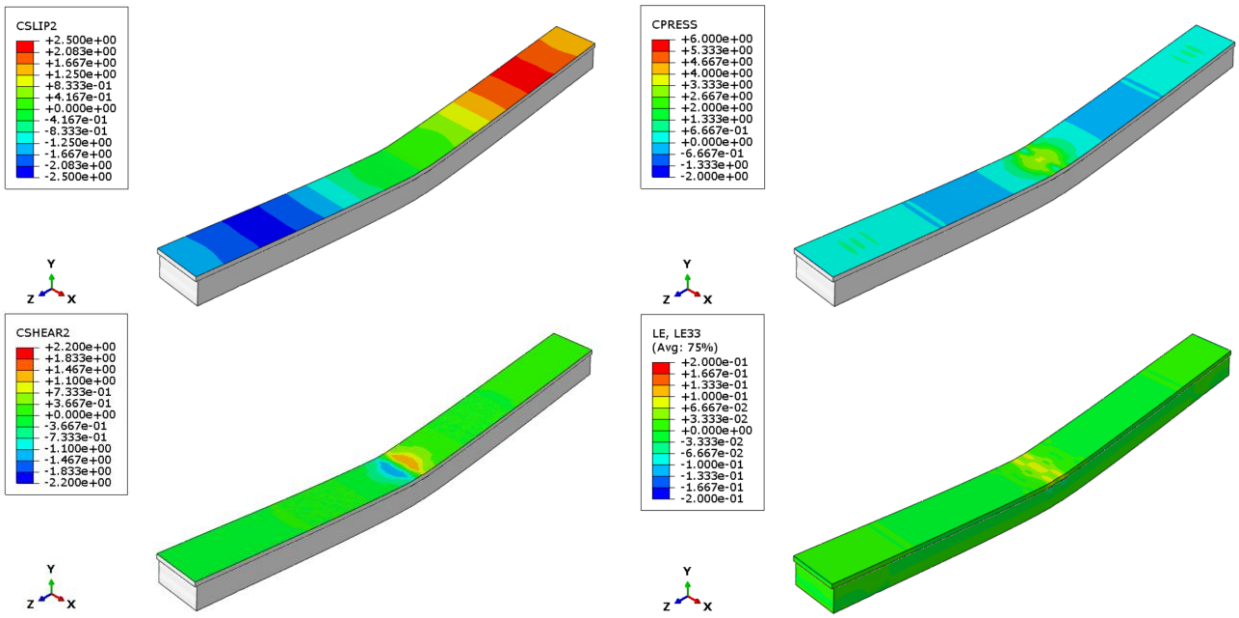

Figure 8. Trends for CSLIP, CPRESS, CSHEAR and strain values at 40 °C.

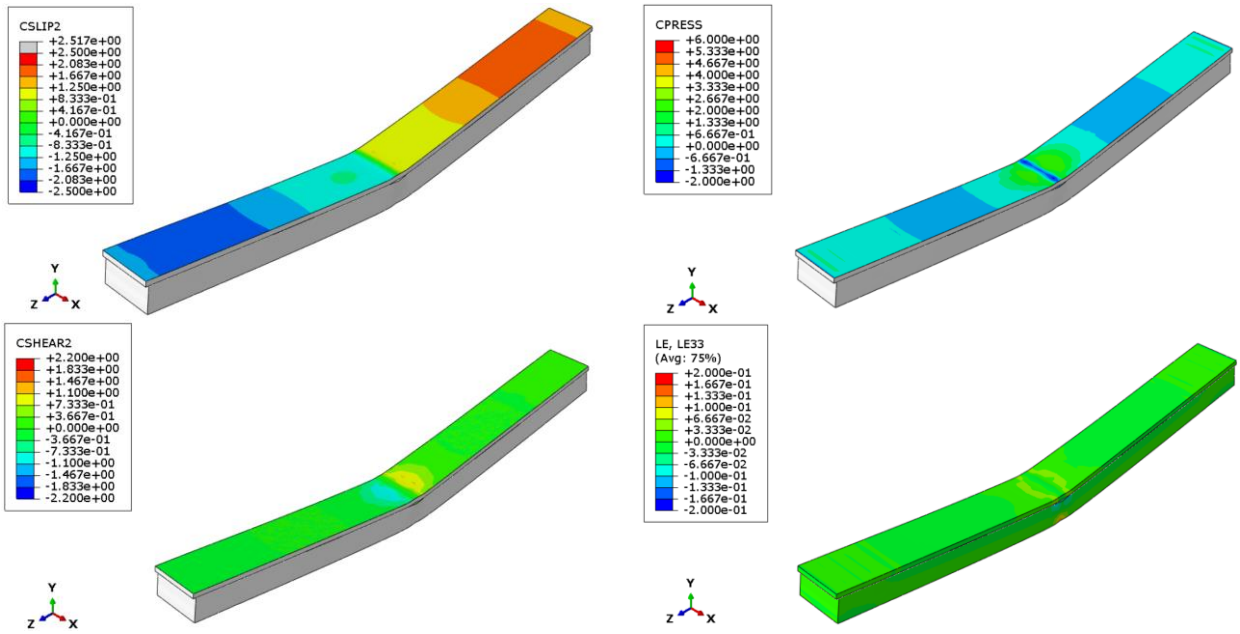

Figure 9. Trends for CSLIP, CPRESS, CSHEAR and strain values at 60 °C.

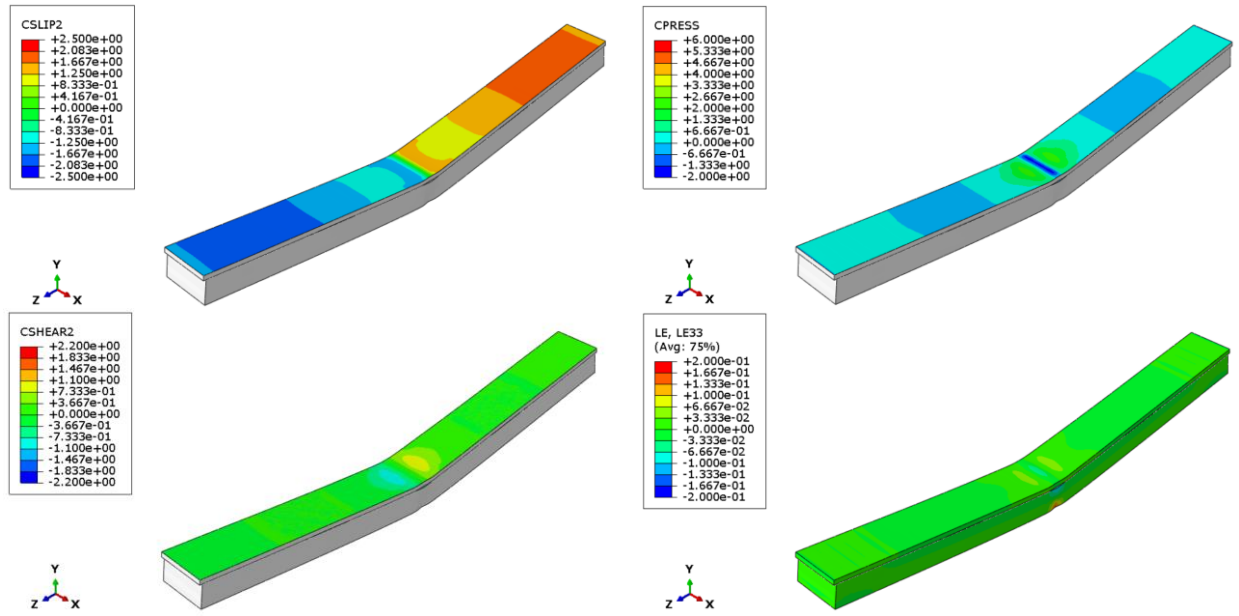

Figure 10. Trends for CSLIP, CPRESS, CSHEAR and strain values at 80 °C.

A relevant aspect that has been assessed is the mutual slippage between wood and polyurethane, which makes it possible to estimate the decay of the adhesive properties between the two materials as the temperature rises. Figure 11 shows the temperature trend of CSHEAR as a function of CSLIP in the z-direction. The curves were obtained by enveloping the minimum and maximum values observed over the entire contact area at the interface. As can be seen, as the test temperature increases, there is a reduction in the frictional stresses (values are negative according to the convention adopted by the software). This reduction in tangential adhesion stress is due to the decay of the mechanical properties of the materials that form the beam. This phenomenon can be attributed to the greater fluidity exhibited by polyurethane at elevated temperatures.

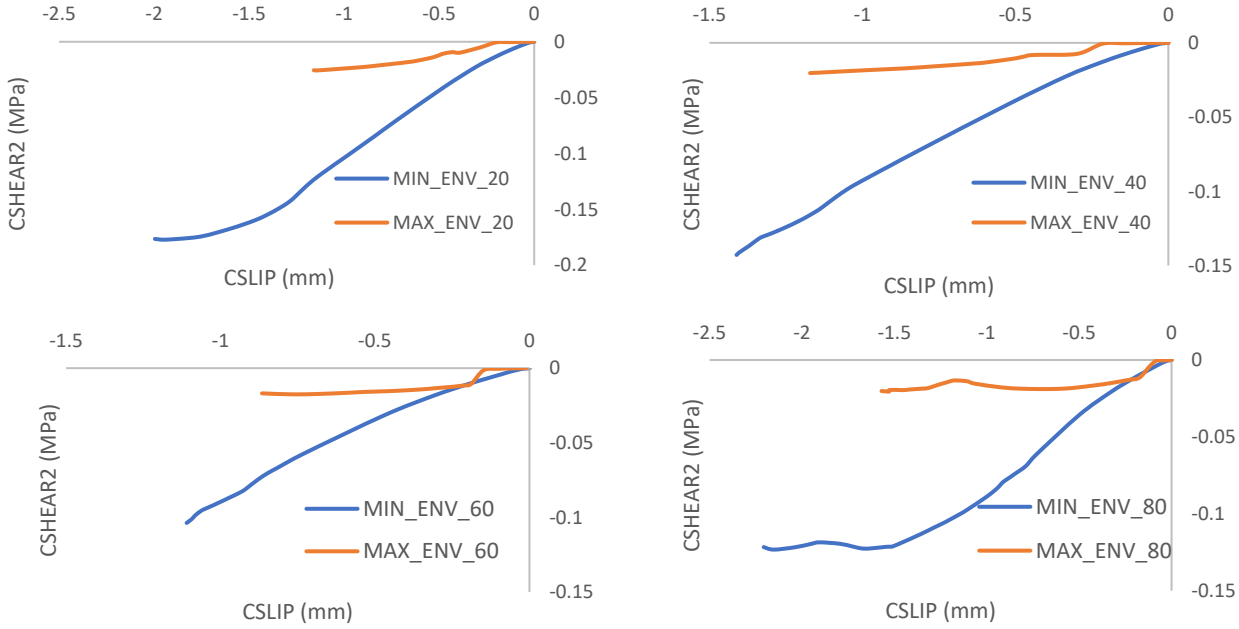

Figure 11. Interface bond constitutive diagrams: maximum and minimum envelopes at 20, 40, 60, and 80 °C are presented.

5. Conclusions

Specifically, in the present work, we were concerned with the definition of a finite element model simulating the thermo-mechanical behavior of a new type of patented polyurethane-based adhesive joints with identification code PL207028 (B1).

Important indications were derived regarding the strongly non-linear behavior exhibited by the materials in combination (wood and polyurethane). The composite beam exhibits a progressive reduction in strength and ultimate deflection with increasing temperature as the mechanical properties of the plastic matrix decay. However, this weakening is not severe enough to be dangerous. Even for the specimens tested at 80 °C, the actual failure always occurred in the wood, although the 4 mm thick specimens experienced delamination phenomena at 80 °C, resulting in greater stress concentration in the underlying wood board. As part of the present work, these experimental results were used to create a finite element model that would allow the experimental test to be simulated in a numerical environment. This was for the dual purpose of being able to expand the case study and to investigate the behavior at the wood–polyurethane interface. This second aspect is of extreme interest, since this kind of interaction is difficult to monitor in the laboratory, without going on to create relevant disturbance phenomena on the final result of the test. The model was built using the micro-modeling strategy, in which each material was defined by means of brick elements. In addition, mechanical properties were defined for each material in detail, so that wood precisely simulates real anisotropic behavior, while polyurethane exactly follows commonly adopted hyperelastic constitutive bonds. The curves found by numerical analysis showed a deviation of less than 10% for each of the cases observed.

On the basis of bending tests and numerical analyses, it was observed that the strength of beams is strictly related to the shear strength of the adhesive. In fact, the polyurethane layer goes through delamination phenomena, resulting in a sudden loss of load redistribution, which is its main advantage under optimal operating conditions. It has also been observed that, as temperature increases, the load-bearing capacity of the laminated beam in bending decreases. The decreases between 20 °C and 80 °C are 38.6%, 43.8% and 41.55% for t = 1, 2 and 4 mm, respectively.

Experimental tests have also shown that greater adhesive thicknesses provide greater adhesion and allow greater displacements before reaching the failure limit value. In

addition, this type of flexible joint did not show an excessive reduction in elasticity with increasing temperature and thickness, providing a potentially ideal tool for design. The disadvantage, however, is the degradation phenomena that the material appears to undergo upon prolonged exposure to high temperatures, resulting in a loss of tensile strength of nearly 35%.

The proposed numerical model was calibrated based on the available experimental data. The FE model has been realized according to the detailed micro-modeling approach, considering all the non-linearities that characterize the problem:

- anisotropic behavior of the wood;
- hyperelastic behavior of the polyurethane;
- attritive/fragile behavior at the wood-polyurethane interface;
- combined thermal and mechanical loading.

Numerical results proved to be extremely accurate in simulating the test performed, providing results that always adhered to those obtained experimentally. From the numerical model it was possible to derive important indications of the stress trend at the interface between wood and polyurethane, as well as to monitor the relative displacements between the contacting faces.

The numerical model made it possible to:

- observe the loss of adhesion stress between wood and polyurethane along heating processes;
- evaluate the difference in CSHEAR between 20 and 80°, resulted in 20% for the maximum envelope and 30% for the minimum envelope;
- identify a correlation between the adhesion stress and the mutual slip of the contacting surfaces, which is fundamental for determining an equivalent stiffness for this type of constraint;
- evaluate the deformation state of the adhesive layer at the interface with temperature changes.

The results obtained proved to be extremely useful in describing the frictional behavior between polyurethane and wood, providing a basis for optimizing this type of joint.

The methodology proposed has the great advantage of being general, since it can be applied to all cases of composite materials consisting of several contact layers. Its application can be imagined in the case of other types of plastic joints (adhesive and non-adhesive) for wooden structures, as well as in the case of totally different elements, such as fiber mesh reinforcements, glass–cement structures and others.

A next step will be to update the case study, applying the joint to a complete structure and evaluating the global behavior.

6. Patents

Patent nr PL207028 (B1): *Method of making the load-bearing repair joints of set mechanical parameters in concrete and masonry building structures*, protected by the Owner as the patent No. PL207028 (B1) granted by the Patent Office of the Republic of Poland and announced on 29 October 2010 WUP 10/10, as a result of patent application P-370025 submitted to the Patent Office of the Republic of Poland on 10 September 2004 and implemented on the basis of the granting of the full and exclusive license to FlexAndRobust Sp. z o.o. by the Cracow University of Technology.

Author Contributions: Conceptualization, A.L.S., K.Ś.-W. and F.R.; methodology, A.L.S.; software, A.L.S. and F.R.; formal analysis, A.L.S. and M.F.S.; investigation, K.Ś.-W., M.F.S. and B.Z.; writing—original draft preparation, A.L.S.; writing—review and editing, A.L.S., M.F.S. and K.Ś.-W. All authors have read and agreed to the published version of the manuscript.

Funding: This work was supported by Research Grants from the Faculty of Civil Engineering at Cracow University of Technology.

Institutional Review Board Statement: Not applicable.

Informed Consent Statement: Not applicable.

Data Availability Statement: The data presented in this study are available on request from the corresponding author. The data are not publicly available due to privacy.

Conflicts of Interest: The authors declare no conflicts of interest.

References

1. Banea, M.D.; da Silva, L.F.M. Adhesively Bonded Joints in Composite Materials: An Overview. *Proc. Inst. Mech. Eng. Part L J. Mater. Des. Appl.* **2009**, *223*, 1–18. [CrossRef]
2. Bedon, C.; Reynolds, T.; Aloisio, A.; Bader, T.; Buka-Vaivade, K.; Caprio, D.; Ceylan, A.; Celis, R.; Chocholaty, B.; De Santis, Y.; et al. *HELEN WG2: Design of Taller Timber Buildings against Deformations and Vibrations: A State-of-the-Art Review*; ResearchGate: Berlin, Germany, 2022.
3. Ber, B.; Finžgar, G.; Premrov, M.; Štrukelj, A. On Parameters Affecting the Racking Stiffness of Timber-Glass Walls. *Glass Struct. Eng.* **2019**, *4*, 69–82. [CrossRef]
4. Štrukelj, A.; Ber, B.; Premrov, M. Racking Resistance of Timber-Glass Wall Elements Using Different Types of Adhesives. *Constr. Build. Mater.* **2015**, *93*, 130–143. [CrossRef]
5. Shirmohammadli, Y.; Pizzi, A.; Raftery, G.M.; Hashemi, A. One-Component Polyurethane Adhesives in Timber Engineering Applications: A Review. *Int. J. Adhes. Adhes.* **2023**, *123*, 103358. [CrossRef]
6. Clau, S.; Dijkstra, D.J.; Gabriel, J.; Kläusler, O.; Matner, M.; Meckel, W.; Niemz, P. Influence of the Chemical Structure of PUR Prepolymers on Thermal Stability. *Int. J. Adhes. Adhes.* **2011**, *31*, 513–523. [CrossRef]
7. Li, Y.F.; Xie, Y.M.; Tsai, M.J. Enhancement of the Flexural Performance of Retrofitted Wood Beams Using CFRP Composite Sheets. *Constr. Build. Mater.* **2009**, *23*, 411–422. [CrossRef]
8. Jasieńko, J.; Nowak, T.P. Solid Timber Beams Strengthened with Steel Plates—Experimental Studies. *Constr. Build. Mater.* **2014**, *63*, 81–88. [CrossRef]
9. Radford, D.W.; Van Goethem, D.; Gutkowski, R.M.; Peterson, M.L. Composite Repair of Timber Structures. *Constr. Build. Mater.* **2002**, *16*, 417–425. [CrossRef]
10. Kwiecień, A.; de Felice, G.; Oliveira, D.V. Repair of Composite-to-Masonry Bond Using Flexible Matrix. *Mater. Struct.* **2016**, *49*, 2563–2580. [CrossRef]
11. Kwiecień, A.; Rodacki, K.; Zając, B.; Tomasz, K. Mechanical Behavior of Polyurethane Adhesives Applied to Timber Joints in Repair of Historical Timber Structures. In *Structural Analysis of Historical Constructions*; RILEM Bookseries; Springer: Cham, Switzerland, 2019; Volume 18, pp. 1603–1612. [CrossRef]
12. Huang, S.; Bachtiar, E.V.; Yan, L.; Kasal, B. Bond Behaviour and Thermal Stability of Flax/Glass Hybrid Fibre Reinforced Polymer–Timber Structures Connected by Polyurethane. *Constr. Build. Mater.* **2022**, *322*, 126456. [CrossRef]
13. Vallée, T.; Correia, J.R.; Keller, T. Optimum Thickness of Joints Made of GFPR Pultruded Adherends and Polyurethane Adhesive. *Compos. Struct.* **2010**, *92*, 2102–2108. [CrossRef]
14. Liao, L.; Huang, C.; Sawa, T. Effect of Adhesive Thickness, Adhesive Type and Scarf Angle on the Mechanical Properties of Scarf Adhesive Joints. *Int. J. Solids Struct.* **2013**, *50*, 4333–4340. [CrossRef]
15. Kläusler, O.; Clauß, S.; Lübke, L.; Trachsel, J.; Niemz, P. Influence of Moisture on Stress–Strain Behaviour of Adhesives Used for Structural Bonding of Wood. *Int. J. Adhes. Adhes.* **2013**, *44*, 57–65. [CrossRef]
16. Bomba, J.; Šedivka, P.; Böhm, M.; Devera, M. Influence of Moisture Content on the Bond Strength and Water Resistance of Bonded Wood Joints. *BioRes* **2014**, *9*, 5208–5218. [CrossRef]
17. Lettieri, M.; Frigione, M. Effects of Humid Environment on Thermal and Mechanical Properties of a Cold-Curing Structural Epoxy Adhesive. *Constr. Build. Mater.* **2012**, *30*, 753–760. [CrossRef]
18. Moussa, O.; Vassilopoulos, A.P.; de Castro, J.; Keller, T. Time–Temperature Dependence of Thermomechanical Recovery of Cold-Curing Structural Adhesives. *Int. J. Adhes. Adhes.* **2012**, *35*, 94–101. [CrossRef]
19. Zając, B. *Rigid and Flexible Shear Adhesive Connections Working at Elevated Temperature*; Wydawnictwo Politechniki Krakowskiej: Kraków, Poland, 2018.
20. Goland, M.; Reissner, E. The Stresses in Cemented Joints. *J. Appl. Mech.* **2021**, *11*, A17–A27. [CrossRef]
21. Da Silva, L.F.M.; das Neves, P.J.C.; Adams, R.D.; Spelt, J.K. Analytical Models of Adhesively Bonded Joints—Part I: Literature Survey. *Int. J. Adhes. Adhes.* **2009**, *29*, 319–330. [CrossRef]
22. Da Silva, L.F.M.; das Neves, P.J.C.; Adams, R.D.; Wang, A.; Spelt, J.K. Analytical Models of Adhesively Bonded Joints—Part II: Comparative Study. *Int. J. Adhes. Adhes.* **2009**, *29*, 331–341. [CrossRef]
23. Vidholdová, Z.; Ciglian, D.; Reinprecht, L. Bonding of the Thermally Modified Norway Spruce Wood with the Pur and Pvac Adhesives. *Acta Fac. Xylologiae Zvolen* **2021**, *63*, 63–73. [CrossRef]
24. Zhang, R.; Dai, H.; Smith, G.D. Investigation of the High Temperature Performance of a Polyurethane Adhesive Used for Structural Wood Composites. *Int. J. Adhes. Adhes.* **2022**, *116*, 102882. [CrossRef]
25. Verdet, M.; Salenikovich, A.; Cointe, A.; Coureau, J.-L.; Galimard, P.; Toro, W.M.; Blanchet, P.; Delisee, C. Mechanical Performance of Polyurethane and Epoxy Adhesives in Connections with Glued-in Rods at Elevated Temperatures. *Bioresources* **2016**, *11*, 8200–8214. [CrossRef]

26. Voß, M.; Evers, T.; Vallée, T. Low-Temperature Bonding of Timber Structures. In Proceedings of the 13th World Conference on Timber Engineering, WCTE 2023, Oslo, Norway, 19–22 June 2023; Volume 1, pp. 339–344.
27. Kwiecień, K.; Śliwa Wieczorek, K.; Rizzo, F.; Kwiecień, A.; Zając, B.; Rutkowski, P.; Szumera, M.; Berezicka, A.; Kwiecień, K.; Kwiecień, A.; et al. Thermal Characteristics of Polyurethanes for Joints Applications of Wooden Structures. In Proceedings of the International Conference on Wood Adhesives 2022, Portland, OR, USA, 11–13 May 2022; Bedon, C., Ed.; Forest Products Society (FPS): LaGrange, GA, USA, 2022; Volume 1, pp. 1108–1117.
28. Davis, G. The Performance of Adhesive Systems for Structural Timbers. *Int. J. Adhes. Adhes.* **1997**, *17*, 247–255. [CrossRef]
29. Kwiecień, K.; Kwiecień, A.; Stryszewska, T.; Szumera, M.; Dudek, M. Durability of PS-Polyurethane Dedicated for Composite Strengthening Applications in Masonry and Concrete Structures. *Polymers* **2020**, *12*, 2830. [CrossRef] [PubMed]
30. Clauss, S.; Joák, M.; Niemz, P. Thermal Stability of Glued Wood Joints Measured by Shear Tests. *Eur. J. Wood Wood Prod.* **2011**, *69*, 101–111. [CrossRef]
31. Zhang, Y.; Zhou, Z.; Tan, Z. Compression Shear Properties of Bonded–Bolted Hybrid Single-Lap Joints of C/C Composites at High Temperature. *Appl. Sci.* **2020**, *10*, 1054. [CrossRef]
32. Çitil, Ş. Experimental and Numerical Investigation of Adhesively Bonded Curved Lap Joints under Three-Point Bending. *Mechanics* **2019**, *24*, 824–832. [CrossRef]
33. Fecht, S.; Vallée, T.; Tannert, T.; Fricke, H. Adhesively Bonded Hardwood Joints under Room Temperature and Elevated Temperatures. *J. Adhes.* **2014**, *90*, 401–419. [CrossRef]
34. Śliwa-Wieczorek, K.; Zając, B. Rigid and Flexible Double Shear Lap Adhesive Joint at Elevated Temperature—An Experimental Study. *Polymers* **2021**, *13*, 2873. [CrossRef]
35. Krzyżaniak, Ł.; Kuşkun, T.; Kasal, A.; Smardzewski, J. Analysis of the Internal Mounting Forces and Strength of Newly Designed Fastener to Joints Wood and Wood-Based Panels. *Materials* **2021**, *14*, 7119. [CrossRef]
36. Śliwa-Wieczorek, K.; Zając, B. PUFJ (PolyUrethane Flexible Joints) as an Innovative Polyurethane System for Structural and Non-Structural Bonding of Timber Elements. *J. Phys. Conf. Ser.* **2023**, *2423*, 12015. [CrossRef]
37. Imakawa, K.; Ochiai, Y.; Aoki, K.; Hori, N.; Takemura, A.; Yamaguchi, T. Mechanical Properties of Hybrid Joints in Timber Structures. *J. Wood Sci.* **2022**, *68*, 37. [CrossRef]
38. *ISO 13061-3:2014*; Physical and Mechanical Properties of Wood Test Methods for Small Clear Wood Specimens Part 3: Determination of Ultimate Strength in Static Bending. ISO: Geneva, Switzerland, 2014.
39. *ISO 13061-4:2014*; Physical and Mechanical Properties of Wood Test Methods for Small Clear Wood Specimens Part 4: Determination of Modulus of Elasticity in Static Bending. ISO: Geneva, Switzerland, 2014.
40. *ASTM D143-22*; Standard Test Methods for Small Clear Specimens of Timber. ASTM: West Condhohocken, PA, USA, 2022.
41. *ISO 10365:1998*; Adhesives—Designation of Main Failure Patterns. ISO: Geneva, Switzerland, 1998.
42. *EN 408:2012*; Timber Structures—Structural Timber and Glued Laminated Timber—Determination of Some Physical and Mechanical Properties. European Standards: Pilsen, Czech Republic, 2012.
43. Stamer, J. Elastizitatsuntersuchungen an Holzern (Elasticity Tests on Wood). *Ing.-Arch.* **1935**, *6*, 1–8. [CrossRef]
44. Dahl, K.B. Mechanical Properties of Clear Wood from Norway Spruce. Ph.D. Thesis, Norwegian University of Science and Technology, Trondheim, Norway, 2009.
45. Smith, M. *ABAQUS/Standard User's Manual, Version 6.12*; Dassault Systèmes Simulia Corp.: Paris, France, 2009.
46. Pečnik, J.G.; Gavrić, I.; Sebera, V.; Kržan, M.; Kwiecień, A.; Zając, B.; Azinović, B. Mechanical Performance of Timber Connections Made of Thick Flexible Polyurethane Adhesives. *Eng. Struct.* **2021**, *247*, 113125. [CrossRef]

Disclaimer/Publisher's Note: The statements, opinions and data contained in all publications are solely those of the individual author(s) and contributor(s) and not of MDPI and/or the editor(s). MDPI and/or the editor(s) disclaim responsibility for any injury to people or property resulting from any ideas, methods, instructions or products referred to in the content.